



Crystal growth, physical properties, and theoretical investigation on organic acentric single crystal towards efficient second-order NLO applications: Triphenylguanidine

M. S. Kajamuhideen¹ · K. Sethuraman¹ · K. Ramamurthi²

Received: 30 April 2018 / Accepted: 13 October 2018 / Published online: 22 October 2018
© Springer-Verlag GmbH Germany, part of Springer Nature 2018

Abstract

A novel organic nonlinear optical crystal Triphenylguanidine (TPG) was grown by the solvent evaporation method. Single-crystal X-ray diffraction (XRD) studies showed that the TPG compound crystallizes in orthorhombic crystal system with $Pna2_1$ space group and the corresponding lattice planes of reflections were indexed using powder XRD studies. Fourier transform infrared and Fourier transform Raman studies revealed the presence of various functional groups in the TPG crystal. The molecular structure of TPG was also confirmed using the NMR studies. UV–Vis studies validate the aptness of TPG crystal towards nonlinear optical applications. TPG crystal shows blue emission from photoluminescence studies. The mechanical stability of the grown crystal was identified using Vickers microhardness studies. Dielectric studies were carried out as a function of frequency at room temperature. Powder SHG effective nonlinearity of TPG crystal is about 2.3 times that of standard KDP. The thermal stability of TPG crystal was investigated by the TG-DTA studies. Using Gaussian 03 program the HOMO–LUMO energy gap and first-order hyperpolarizability value for TPG molecule were calculated. The calculated first-order hyperpolarizability value of TPG molecule is 17 times that of urea.

1 Introduction

In recent days, photonics are playing a significant role to make our society ultrafast. As a result, photonics are turned into a dynamic field of examination for our modern society. It has been used in diverse fields like data storage, telecommunication, optical switching, and optical signal processing. In this technological era, the design of devices have been modified, so, nowadays, photons are being considered more for broadcasting information rather than taking electrons [1–6]. Due to this reason, there is an increased demand for new and innovative nonlinear optical materials [7]. In earlier days, some of the inorganic materials such as lithium niobate (LiNbO_3) and potassium dihydrogen phosphate (KDP) are mostly considered due to their modest nonlinearity [8]. With

the owned limitations among inorganic materials, organic materials can be tuned for efficient higher order nonlinearity [9]. The second-order nonlinear optical (NLO) effect of certain organic noncentrosymmetric materials shows the improved results compared to that of inorganic materials [10, 11]. Fast response time, high NLO competency and lofty optical damage threshold are some of the advantages offered by organic materials over inorganic NLO materials [12, 13]. Organic materials showing quadratic nonlinear optical properties have received considerable attention over past 3 decades due to their potential applications in optical signal processing [14, 15].

The organic compounds of Guanidines exhibit significant biological and chemical properties [16]. Furthermore, guanidine and their derivatives are considered to be potentially interesting materials for quadratic NLO applications as demonstrated by Zyss et.al. [17, 18]. Triphenylguanidine (TPG) a derivative of guanidine compounds has three electron donor atoms two amino nitrogen ($-\text{NH}$) atoms and one imine ($=\text{N}-$) nitrogen atom. The donor ability of the nitrogen centers allows to explore equally the electronic and steric effect stimulated by the variation of organic substituent and by the intra and inter-molecular interactions [19]. The TPG compound is also considered as potentially

✉ K. Sethuraman
sethuraman_33@yahoo.com

¹ School of Physics, Madurai Kamaraj University, Madurai, Tamilnadu 625021, India

² Department of Biomedical Engineering, Aarupadai Veedu Institute of Technology, Vinayaga Mission's Research Foundation, Vinayaga Nagar, Paiyanoor, Tamilnadu 603104, India

significant for quadratic nonlinear optical applications. The donor atom at the centre of the molecule is an advantageous contribution to the enhanced polarizability [20].

Silva et al. reported that the TPG crystal belongs to orthorhombic crystal system which exists in noncentrosymmetric space group $Pna2_1$ whose molecular structure is shown in Fig. 1 [21]. However, the physicochemical attributes of the TPG crystal have not been explored till now, thereby hindering the effective probing of TPG crystals and its consecutive derivative. Therefore, the present work reports the growth of TPG single crystals and investigations onto its optical, thermal, mechanical, and dielectric properties. Concurrently, theoretical values of HOMO–LUMO energy gap and first-order hyperpolarizability were calculated and reported in this work for the first time.

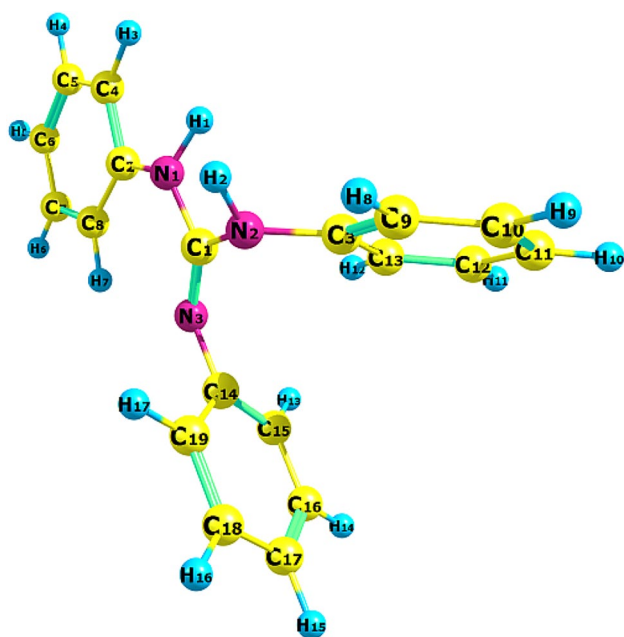


Fig. 1 Molecular structure of TPG

2 Experimental section

2.1 Synthesis

Analytical grade of TPG and ethanol was purchased from Sigma-Aldrich. Required quantity of TPG was dissolved in ethanol solution and stirred well at room temperature for 6 h. Then, the beaker containing solution was covered with polyethylene sheet and pin holes were made on the surface of the sheet. Furthermore, the purity of the synthesized material was improved by repeated recrystallization using ethanol. The recrystallized material with high purity was used for crystal growth process.

2.2 Solubility

The crystal growth rate and, hence, the quality of the crystals depend on the purity of the chemical, solvent, solubility, and temperature. The solubility of TPG was measured in ethanol over the temperature range from 30 to 60 °C in the steps of 5 °C. Initially, a 250 mL capacity glass beaker containing 100 ml of ethanol was placed in an ultra-cryostat temperature bath with a controlled accuracy of ± 0.01 °C and the temperature was set at 30 °C. The powdered sample of TPG was steadily added in ethanol and stirred using magnetic stirrer. On attaining the saturation, the equilibrium concentration of the solution was analyzed gravimetrically. The same procedure was repeated for temperatures 35, 40, 45, 50, 55, and 60 °C to estimate the amount of TPG required to saturate the solution at various temperatures. The solubility graph drawn for TPG is shown in Fig. 2(a). From the figure, it is observed that the solubility of TPG increases with increase in temperature, which illustrates that the material exhibits positive solubility temperature gradient.

2.3 Crystal growth and morphology

The saturated solution of TPG was prepared in ethanol at 30 °C with the help of solubility data (2.383 g/100 mL).

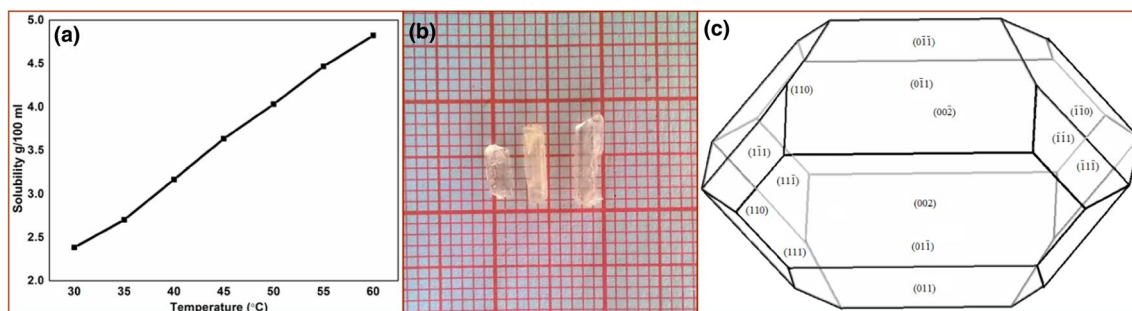


Fig. 2 a Solubility curve of TPG. b Grown TPG crystal. c BFDH morphology diagram of TPG crystal

The prepared solution was filtered and transferred to a glass beaker and tightly covered with aluminum foil with a few small holes to enable the evaporation of the solvent at room temperature and kept in a vibration-free environment. The first speck of nucleation occurs in about 10 days. The colorless and optically transparent quality crystal was harvested from the parent solution in a period of 30 days. Figure 2b shows the as-grown TPG single crystals. The morphology of the grown TPG crystal was indexed by Bravais–Friedel–Donnay–Harker (BFDH) Model [22, 23] using mercury software in which the respective crystallographic information file (CIF) was used as input. The predicted morphology is found to be comparable with the morphology of highly transparent grown TPG crystal. The TPG crystal has 14 well-developed faces and the indexed crystallographic faces are shown in Fig. 2c.

3 Results and discussion

3.1 Single-crystal and powder X-ray diffraction analysis

Optical quality single crystal of TPG was subjected to single-crystal XRD studies using an Enraf–Nonius CAD4 diffractometer with Mo K_{α} ($\lambda = 0.7107 \text{ \AA}$) radiation at room temperature. The unit cell parameters of the crystal obtained are $a = 9.226(8) \text{ \AA}$, $b = 10.843(8) \text{ \AA}$, $c = 16.374(4) \text{ \AA}$, $\alpha = \beta = \gamma = 90^\circ$, and $V = 1638(4) \text{ \AA}^3$. The TPG was found to crystallize with noncentrosymmetric space group $Pna2_1$, which is an important requirement for the second-harmonic generation. The obtained results were found to match well with the reported data. Table 1 shows the comparison between the obtained single-crystal XRD data values and the reported values [21].

Powder X-ray diffraction (PXRD) pattern for TPG is analyzed using PAN analytical X-pert pro diffractometer with Cu K_{α} radiation ($\lambda = 1.5407 \text{ \AA}$). Figure 3a shows the Powder X-ray diffraction pattern obtained experimentally, whereas

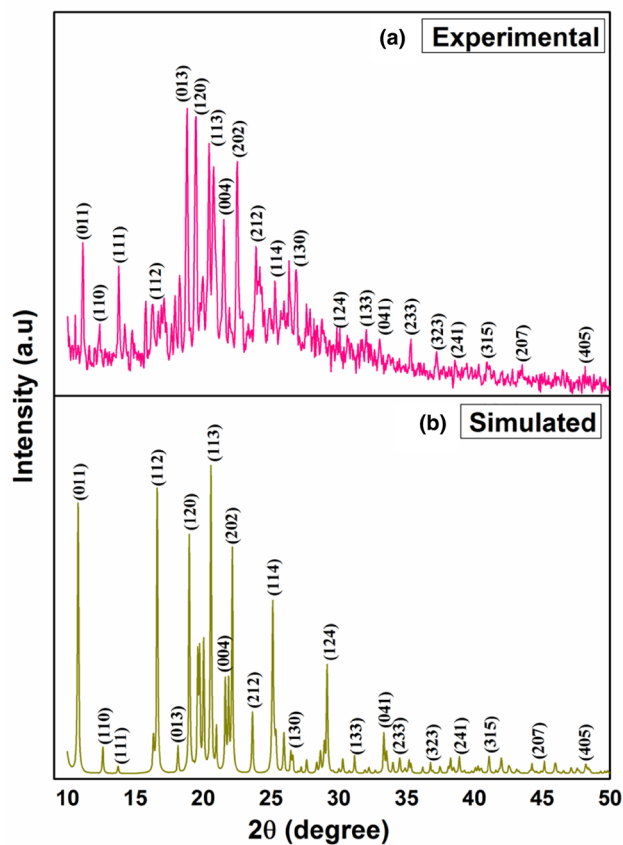


Fig. 3 a Experimental and b simulated powder XRD patterns of TPG

Fig. 3b shows the PXRD obtained theoretically using the MERCURY software for TPG. The various planes of reflections in PXRD were also indexed with the help of the same software [24]. From the figures, it could be seen that both the simulated and experimental patterns are in close agreement with each other.

3.2 Vibrational analysis

The Fourier transform infrared (FT-IR) spectrum of TPG powder sample was recorded using the Shimadzu IR Affinity (FT-IR spectrophotometer) in the frequency range from 4000 to 400 cm^{-1} with the resolution of 0.5 cm^{-1} . FT-Raman spectrum was recorded using BRUKER RFS27: stand-alone FT-Raman spectrophotometer and Nd: YAG laser source ($\lambda = 1064 \text{ nm}$) in the spectral range of 3500 – 350 cm^{-1} . FT-IR and FT-Raman spectra of the powder TPG recorded at room temperature which is shown in Figs. 4 and 5 respectively. NH_2 asymmetric stretching mode appeared as a broad band at 3327 cm^{-1} in IR spectrum. The broad IR peak at 3248 cm^{-1} and a weak peak at 3261 cm^{-1} in Raman spectrum is ascribed to symmetric NH_2 stretching vibrations. C-N stretching mode occurs

Table 1 Lattice parameters of Triphenylguanidine single crystals

Parameter	Silva et al. [17]	Present result
a (\AA)	9.226 (8)	9.1975 (3)
b (\AA)	10.843 (8)	10.849 (4)
c (\AA)	16.374 (4)	16.418 (6)
α	90.00°	90.00°
β	90.00°	90.00°
γ	90.00°	90.00°
Volume (\AA^3)	1638(4)	1638.3(1)
System	Orthorhombic	Orthorhombic
Space group	$Pna2_1$	$Pna2_1$

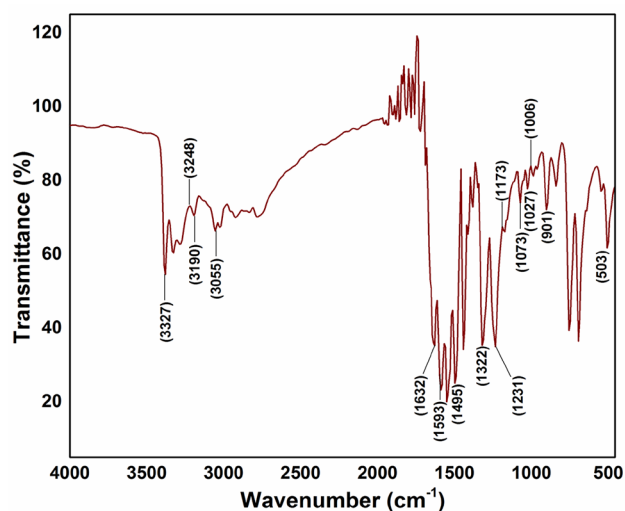


Fig. 4 FT-IR spectrum of TPG crystal

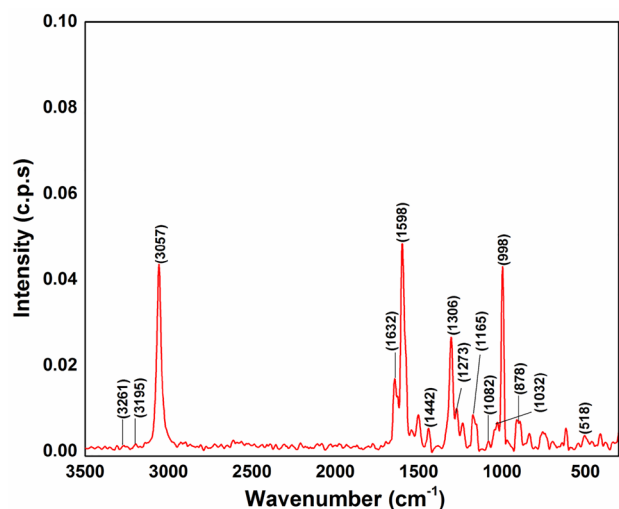


Fig. 5 FT-Raman spectra of TPG crystal

as a medium IR peak at 1632 cm^{-1} and a sharp peak at 1643 cm^{-1} in Raman spectrum. CN_3 symmetric stretching vibration is observed as a very high intense peak at 998 cm^{-1} in Raman spectrum and the corresponding IR peak occurred at 1006 cm^{-1} . The band at 3190 cm^{-1} in IR spectrum is due to NH out-of-plane stretching vibrations and Raman spectrum of this vibration observed at 3195 cm^{-1} . The strong IR peak at 1593 cm^{-1} is attributed to NH_2 -bending vibration. The corresponding vibration in Raman spectrum is appeared as a sharp peak at 1598 cm^{-1} . The band at 1073 cm^{-1} and 1082 cm^{-1} in IR and Raman spectrum, respectively, is ascribed to NH_2 rocking in-plane vibrations. The bands at 1231 cm^{-1} and 1273 cm^{-1} have been assigned to NH asymmetric deformations in FT-IR and Raman spectrum, respectively. NH wagging frequency

is observed at 503 cm^{-1} in FT-IR and at 518 cm^{-1} in FT-Raman [25, 26].

The phenyl ring present in the TPG compound is confirmed on the basis of C–C and C–H vibrations. In the present study, C–H-bending vibration observed at 1027 cm^{-1} in FT-IR and at 1032 cm^{-1} in FT-Raman. C–H stretching vibration occurs at 3055 cm^{-1} in FT-IR spectrum. The Raman counter part of this vibration occurred as a high intense peak at 3057 cm^{-1} . The C–H in-plane and out-of-plane bending vibrations are occurred at 1173 cm^{-1} and 901 cm^{-1} , respectively, in FT-IR spectrum, whereas the corresponding frequencies in Raman spectrum appear at 1165 cm^{-1} and 878 cm^{-1} . The bands at 1495 cm^{-1} and 1442 cm^{-1} have been assigned to C–H deformations in FT-IR and FT-Raman spectrum, respectively. The C–C stretching mode occurs at 1322 cm^{-1} in FT-IR spectrum and the corresponding band appears at 1306 cm^{-1} in Raman spectrum [27]. The characteristic peaks and the corresponding vibrations for the grown TPG crystal have been confirmed via/using FT-IR and FT-Raman spectrometers.

3.3 NMR spectral analysis

The nuclear magnetic resonance (NMR) spectral studies are important analytical technique used to study the structure of organic compounds. In the present study, the ^1H and ^{13}C NMR spectrum were recorded using Bruker 300 MHz spectrometer in a Deuterated DMSO solvent to confirm the molecular structure of TPG compound. The recorded ^1H NMR spectrum is shown in Fig S1(a). The ^1H NMR clearly shows that the compound contains only aromatic protons, because all the protons appeared in the region of above 7 ppm. Furthermore, the NMR spectrum shows five set of protons in which three sets of protons from phenyl protons and the remaining two sets belong to amine protons. The appearance of singlet at 7.97 ppm and 8.75 ppm indicates the presence of two amine protons.

Similarly, the ^{13}C NMR spectrum also confirms the structure of the compound as shown in Fig S1(b). Thus, ^{13}C NMR spectrum reveals that the compound contains only aromatic carbon (the guanidine carbon will also appear in aromatic region).

3.4 Optical transmittance

The optical transmittance plays a major role in identifying the potential NLO material, because a particular material can be of practical use only if it possesses large transparency window without absorption around the fundamental and second-harmonic wavelength. The material with lower cut-off wavelength below 400 nm is essential for the realization of second-harmonic generation (SHG) output in this range using solid-state lasers and diode [28]. The optical

transmittance spectrum of TPG crystal was recorded using SHIMADZU UV–Vis–NIR spectrophotometer in the range of 190 to 900 nm at room temperature. A TPG crystal of thickness 1 mm was used to record the transmittance spectrum and is shown in Fig. 6a. The TPG crystal has transmittance of about 95% in the 350–900 nm range with the cut-off wavelength at 336 nm. The crystal is highly transparent in the entire visible and near-IR region which confirms its candidature for efficient NLO applications. The measured transmittance T was used to find the absorption coefficient (α) using the following formula:

$$\alpha = \frac{2.303 \log \left(\frac{1}{T} \right)}{t}, \quad (1)$$

where T is the transmittance and t is the sample thickness. The optical bandgap of TPG can be acquired from the absorption coefficient (α) using the relation:

$$(\alpha h\nu)^2 = A(E_g - h\nu), \quad (2)$$

where ‘ A ’ is a constant, ‘ E_g ’ is the optical bandgap, ‘ h ’ is the Planck’s constant, and ‘ ν ’ is the frequency of the incident photons. The plot drawn between the variation of $(\alpha h\nu)^2$ and $h\nu$ and the bandgap was estimated by extrapolating the linear portion (Fig. 6b) near the onset of absorption edge. The obtained band-gap energy of TPG is 2.7 eV.

3.5 Photoluminescence studies

Photoluminescence (PL) spectroscopy, a nondestructive technique, used for characterizing vacancies, defects, and other imperfections existing in the single crystals [29]. In recent days, luminescent materials are receiving more attention due to their diverse applications in photochemistry, chemical sensors,

and light-emitting diodes [30]. The luminescent process is due to the excitation of materials by a beam of light which leads to the creation of an electron–hole pair and its recombination emits a photon [31]. The photoluminescence spectrum was recorded using Perkin Elmer spectrofluorometer (Model: LS 45) at room temperature. Figure 7 shows the PL emission spectrum of TPG crystal recorded in the range of 300 to 500 nm with an excitation wavelength of 350 nm. The PL emission peak is observed at 424 nm which gives rise to blue light emission. The sharp emission peak confirms the high crystalline nature of TPG crystal. The band-gap energy of TPG is calculated using the wavelength to energy conversion relation as follows:

$$E_g = \frac{hc}{\lambda e}, \quad (3)$$

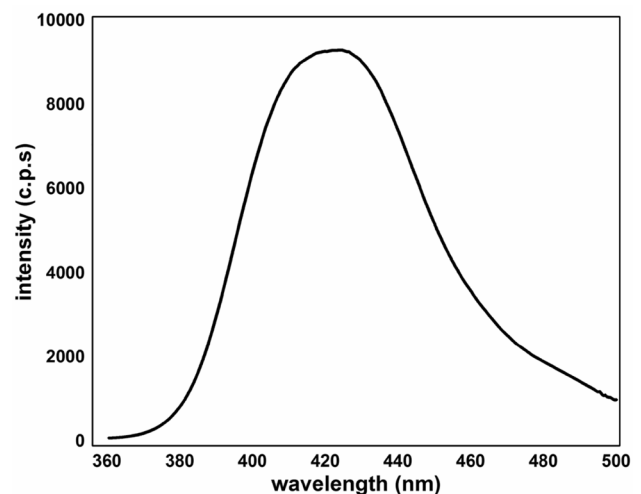


Fig. 7 PL emission spectrum of TPG crystal

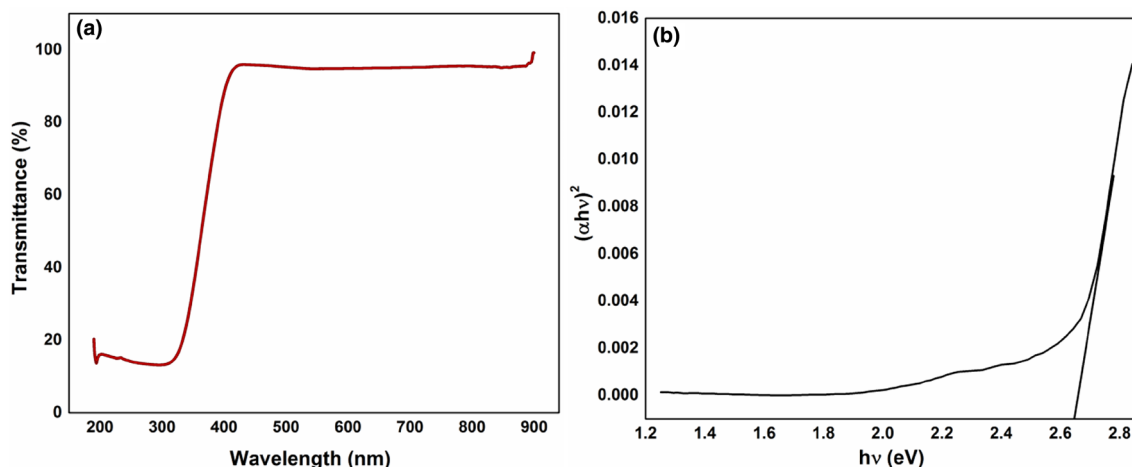


Fig. 6 a UV–Vis transmittance spectrum of TPG crystal. b Bandgap of TPG crystal

where λ is the wavelength of absorbed fluorescence; h , c , and e are constants. From the above relation, band-gap energy of TPG crystal is 2.9 eV. Thus, the grown crystal has blue light emission, and hence, it may be used for optical applications [32].

3.6 Microhardness studies

Microhardness testing is one of the important studies which give the mechanical properties of the crystal [33]. Crystals with good optical property with a better mechanical behavior are especially needed for opto-electronic device fabrications. The mechanical properties of crystalline materials, especially hardness, depend on the structure and crystallographic face of a crystal as well as nature of the chemical bonds. With an increase in temperature, the lattice thermal vibrations will get amplified, which, in turn, modify the lattice energy and decrease the curvature of the potential energy curve [34]. The microhardness studies for TPG crystal has been performed using MATSUZAWA MMTX-7 microhardness tester with a varying load from 10 to 100 g for an indentation time of 5 s at room temperature. The Vicker's microhardness number (H_v) was calculated using the relation:

$$H_v = \frac{1.8554 P}{d^2} \quad (\text{kg/mm}^2), \quad (4)$$

where d is the diagonal length of indenter impression in millimeter, P is the applied load in kilogram, and 1.8544 is the geometrical factor constant for diamond pyramid indenter. Figure 8a shows that the hardness number increases with increasing load [35]. This situation is known as the reverse indentation size effect (RISE) which shows that the crystal possesses superior mechanical strength. When the load is increased above 100 g, cracks were generated on the surface of the crystal due to the release of internal fatigue developed

during indentation. The relation between load and diagonal length of the indenter is given by Meyer's relation $P = K_1 d^n$, where 'n' is termed as work hardening coefficient. The work hardening coefficient 'n' for TPG crystal has been calculated by plotting the graph between $\log p$ and $\log d$ (Fig. 8b) and it is found to be 3.24. Onitsch et al. pointed out that 'n' value should be more than 1.6 for a soft material and should lie between 1 and 1.6 for a hard material. Thus, the grown TPG crystal belongs to a soft-material category.

3.7 Dielectric studies

Dielectric measurements of TPG crystal were performed using the HIOKI HITESTER MODEL 3532-50 LCR meter. A crystal with thickness of 1 mm was coated with silver paste to obtain a fine conducting surface for dielectric measurements. The dielectric behavior of TPG crystal was obtained in a frequency range from 50 to 1 MHz.

Diverse factors such as ionic, orientation, and electronic and space charge polarization for the applied frequency within the crystals determine their dielectric behavior [36]. The frequency-dependent dielectric constant value of TPG crystal at room temperature is shown in Fig. 9a, since, at lower frequency region, the dielectric constant value become very high due to the space charge polarization. While increasing the frequency, the space charge cannot follow the external applied field, which leads to a decrease in dielectric constant value. The lower dielectric constant value at higher frequency is the most essential property for nonlinear optical applications. The frequency-dependent dielectric loss value of TPG crystal at room temperature is shown in Fig. 9b. The dielectric loss is high when the polarization lags behind their applied electric field. If the dielectric loss value decreases, while increasing the frequency, then this will indicate little dissipation of energy as a heat [37]. Thus, TPG crystal

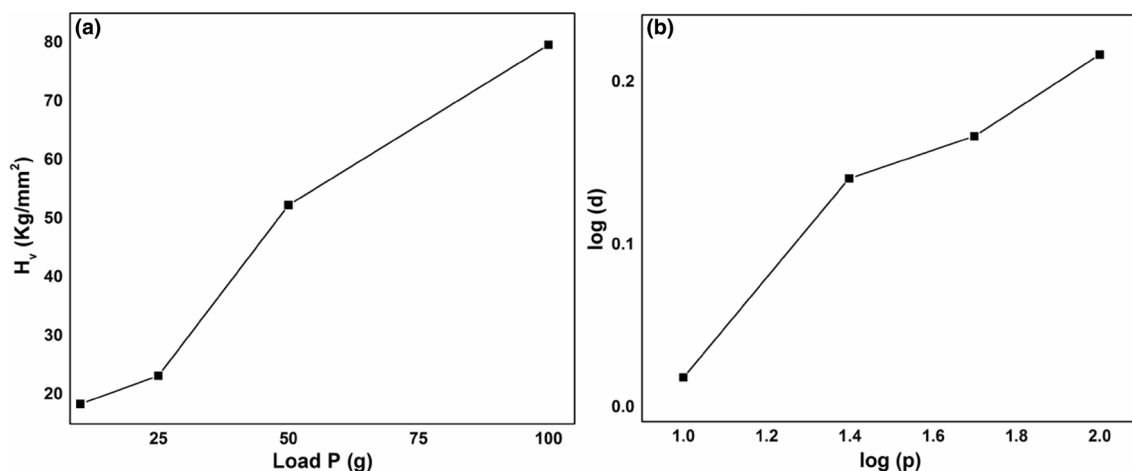


Fig. 8 a Variation of Vickers hardness H_v with load P . b $\log P$ versus $\log d$

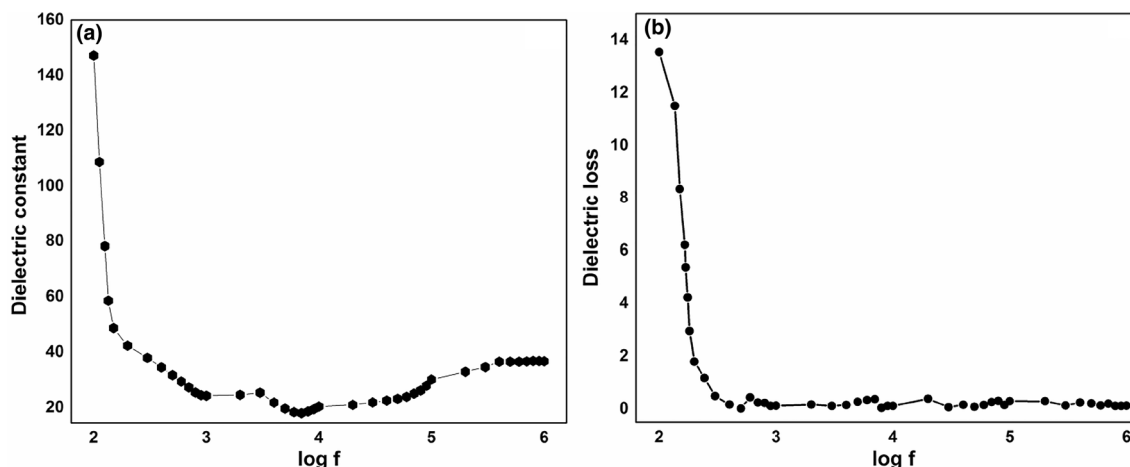


Fig. 9 **a** Dielectric constant of TPG crystal. **b** Dielectric loss of TPG crystal

shows normal dielectric response in the applied frequency range. Several organic crystals and ceramic materials show an anomalous dielectric response to the temperature due to a lofty piezoelectric coefficient [38–41]. The low dielectric loss value designates the absence of defects in TPG crystals. Dielectric studies show that the TPG crystal has good optical quality with lesser defects.

3.8 Second-harmonic generation study

The second-harmonic generation properties of powdered TPG crystal are studied using Kurtz–Perry powder technique [42]. The TPG sample were compactly filled in a micro-capillary tube and then illuminated using Spectra physics Quanta Ray DHS-2 Nd:YAG laser with the first-harmonic output of 1064 nm of pulse width of 8 ns and the repetition rate of 10 Hz. The beam was focused on the TPG sample, and then, output signal of wavelength 532 nm has been generated [43]. The second-harmonic generation property of TPG compound was confirmed by the reduction of input wavelength by half with the emission of green light. The green light intensity has been recorded and converted into an electrical signal using photomultiplier tube and displayed using oscilloscope screen. The SHG efficiency of TPG (28 mV) crystal was found 2.3 times greater than that of reference KDP material (12 mV). The SHG efficiency of powdered TPG was compared with that of some guanidine complex crystals in Table 2.

3.9 Thermal studies

Thermal properties play an important role in utilizing solid-state materials towards various applications. For an NLO crystal, the specific heat and thermal conductivity

Table 2 Compared SHG efficiency for different guanidine compounds

Compound	SHG efficiency (no of times that of KDP)	Reference
Diphenylguanidinium formate	1.8 times	[46]
Diphenylguanidinium perchlorate	1.4 times	[26]
Triphenylguanidine	2.3 times	Present work

can significantly influence the laser-induced damage threshold value for opto-electronic applications [44]. Information about the melting and decomposition point of the materials is important which can be studied by thermogravimetric (TG) and differential thermal analyses (DTA) [45]. The TG-DTA study of TPG samples was performed in a nitrogen atmosphere using a Thermal analyzer SDT Q600 V8.3 instrument with a heating rate of 20 °C min⁻¹ from room temperature to 500 °C. The characteristic TG-DTA curve is shown in Fig. 10. From the TGA curve, it is inferred that the material undergoes a major weight loss at 176 °C, and below this temperature, no weight loss was observed which confirms the absence of physically adsorbed water molecules in the grown crystal. There exists a sharp endothermic peak at 252 °C in DTA curve which is assigned to a major decomposition of the TPG crystal [46]. There exists no evidence of exothermic or endothermic peak present before this decomposition point which indicates the absence of isothermic transition in the TPG crystal [47]. The sharp peak at DTA curve confirms the purity and a better crystalline nature of the grown crystal [48]. The grown TPG crystal can be used for optical device applications up to the range of 176 °C.

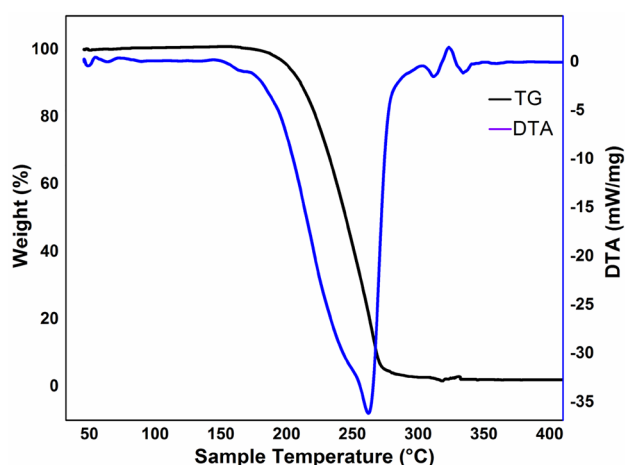


Fig. 10 TG-DTA curve of TPG compound

3.10 HOMO and LUMO studies

HOMO is known as highest molecular orbital having the flexibility to donate an electron to the LUMO, where LUMO is termed as lowest unoccupied molecular orbital having the ability to withdraw an electron from HOMO. The HOMO–LUMO energy gap is directly related to the ionization potential that indicates the chemical reactivity and kinetic stability of a molecule [49, 50]. The molecular structure of TPG was optimized at the DFT/CAMB3LYP method with 6-311++G (d, p) basis set using Gaussian 03 package. The frontier molecular orbital of B2ABP molecule was simulated by gauss view visualizing program. Three-dimensional plot of HOMO–LUMO orbitals of TPG molecule is shown in Fig. 11. The calculated HOMO and LUMO energies are -7.06 eV and -0.05 eV, respectively, and the energy gap of TPG is found to be 7.01 eV. The higher HOMO–LUMO energy gap of TPG shows that the molecule is more stable. The electron affinity and ionization potential of TPG compound could be estimated using HOMO–LUMO energies. Electron affinity (I) is defined as the ability to accept one electron from the donor, so it was obtained from LUMO energy value and the ionization energy (A) has been found from HOMO energy value as follows:

$$I = -E_{\text{HOMO}} \text{ \& } A = -E_{\text{LUMO}} \quad (5)$$

The electronegativity which determines the power of an atom to draw an electron towards itself is calculated from the below equation [51]:

$$\chi = \frac{(I + A)}{2} \quad (6)$$

The chemical hardness of TPG has been calculated using the following equations:

$$\eta = \frac{(I - A)}{2} \quad (7)$$

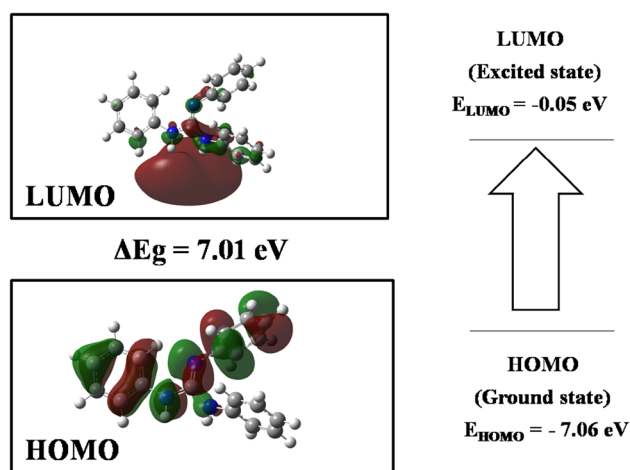


Fig. 11 Atomic orbital compositions of frontier molecular orbital for TPG

The chemical potential which elucidate the escape tendency of electrons from its equilibrium system is given by the following relation:

$$\mu = -\frac{(I + A)}{2} \quad (8)$$

The electrophilicity index of TPG can be calculated using the relation [52]:

$$\omega = \frac{-\chi^2}{2\eta} \quad (9)$$

The calculated values of electronegativity, chemical hardness, chemical potential, and electrophilicity index of TPG molecule were 3.55 , 3.50 , -3.55 , and 1.80 eV, respectively.

3.11 First-order hyperpolarizability calculations

Due to the interaction between the nonlinear optical materials and electromagnetic fields, the nonlinear optical effects in organic molecule increase, which, in turn, produce new fields with altered phase, frequency, amplitude, or other propagation characteristics from the incident field [53]. Theoretical analysis played a vital role in understanding the structure–property relationship assisted in novel nonlinear optical material design. The recognition of NLO property in an organic molecule needs adequate basis sets, and hence, diffusion and polarization functions have to be employed together. As the basis becomes well, one could expect an effective description of the compound and, consequently, more accurate results [43]. In the view of these points, DFT CAMB3LYP method with 6-311++G (d, p) basis sets has been used to study the first-order hyperpolarizability per unit cell volume for TPG molecules.

Table 3 Electric dipole moment (μ), polarizability (α), and first-order hyperpolarizability (β) per unit cell volume of TPG molecule

α Components ($\text{esu} \times 10^{-24}$)		β Components ($\text{esu} \times 10^{-33}$)	
α_{xx}	328.26	β_{xxx}	5193.589
α_{xy}	12.61	β_{xxy}	3275.879
α_{yy}	230.95	β_{xyy}	579.350
α_{xz}	-2.90	β_{yyy}	-238.230
α_{yz}	15.61	β_{xxz}	860.552
α_{zz}	183.77	β_{xyz}	-586.806
α_0	244.73	β_{yyz}	-112.241
Dipole moment (Debye)		β_{xzz}	-317.352
μ_x	0.24	β_{zzz}	-93.244
μ_y	-2.85	β_{zzz}	117.427
μ_z	-1.06	β_{total}	6461.304
μ_0	3.06		

First-order hyperpolarizability is a third-rank tensor with 27 components; the Kleinman symmetry conditions reduced them into ten components [54, 55]. The equations used for the calculating the magnitude of first-order hyperpolarizability from the x , y , and z components are obtained using Gaussian 03 program and it is specified as follows:

$$\beta_{\text{tot}} = (\beta_x^2 + \beta_y^2 + \beta_z^2)^{1/2} \quad (10)$$

The computed electric dipole moment, polarizability and first-order hyperpolarizability per unit cell volume of TPG molecule is depicted in Table 3. The first-order hyperpolarizability value is an essential key factor which is related to NLO properties of the molecule. The first-order hyperpolarizability value of urea molecule was calculated and it is used as a standard reference material for NLO studies. The calculated first-order hyperpolarizability value of TPG molecule (6.461×10^{-30} esu) is 17 times greater than urea molecule (0.379×10^{-30} esu).

4 Conclusions

Optical quality TPG single crystal was grown using solvent evaporation method. XRD and NMR studies confirm the structure of Triphenylguanidine crystal. Vibrational studies were used to identify the various functional groups present in the TPG crystal. The high transparency and low cut-off wavelength obtained from UV-Vis studies authenticate the suitability of a grown crystal towards NLO applications. The grown crystal has a blue emission peak at 424 nm obtained from PL studies. TPG crystal belongs to a soft-material category as acquired from Microhardness studies. The inferior dielectric constant and loss value at higher frequency

make TPG crystal more attractive for opto-electronic and NLO applications. SHG efficiency of TPG crystal is found to be 2.3 times greater than KDP. TG-DTA studies shows that Purity of the grown TPG crystal and its stability has been identified from thermogravimetric analysis. First-order hyperpolarizability and HOMO-LUMO energy gap was theoretically predicted. The grown TPG crystal exhibiting excellent optical activity and enhanced stability confirms its candidature towards efficient electro-optical applications.

References

- H.S. Nagaraja, V. Upadhyaya, P.M. Rao, P.S. Aithal, A.P. Bhatt, *J. Cryst. Growth* **193**, 674–678 (1998)
- M.R.S. Kumar, H.J. Ravindra, A. Jayarama, S.M. Dharmaprakash, *J. Cryst. Growth* **286**, 451–456 (2006)
- P. Srinivasan, M. Gunasekaran, T. Kanagasekaran, R. Gopalakrishnan, P. Ramasamy, *J. Cryst. Growth* **289**, 639–646 (2006)
- N. Vijayan, G. Bhagavannarayana, R.R. Babu, R. Gopalakrishnan, K.K. Maurya, P. Ramasamy, *Cryst. Growth Des.* **6**, 1542–1546 (2006)
- S. Suresh, A. Ramanand, D. Jayaraman, P. Mani, *Rev. Adv. Mater. Sci* **30**, 175–183 (2012)
- D. Xu, M. Xiang, Z. Tan, *Acta Chim. Sin* **41**, 570–573 (1983)
- K. Thukral, N. Vijayan, M. Vij, C.M. Nagaraja, V. Jayaramakrishnan, M.S. Jayalakshmy, R. Kant, *Mat. Chem. Phys* **194**, 90–96 (2017)
- P.S.P. Silva, M.A.P. Goncalves, M.R. Silva, A. Zawadzka, B. Sahraoui, J.A. Paixao, *J. Opt. Mat* **84**, 606–613 (2018)
- V. Nagarajan, A.J.N. Ananth, S. Ramaswamy, *Cryst. Res. Technol.* **53**, 1700217 (2018)
- S.R. Marder, J.W. Perry, W.P. Schaefer, *Science* **245**, 626 (1989)
- P.J. Lacroix, R. Clement, K. Nakatani, J. Zyss, I. Ledoux, *Science* **263**, 658 (1994)
- P.S.P. Silva, C. Cardoso, M.R. Silva, J.A. Paixao, A.M. Beja, M.H. Garcia, N. Lopes, *J. Phys. Chem. A* **114**, 2607–2617 (2010)
- U. Venkataramudu, C. Sahoo, S. Leelashree, M. Venkatesh, D. Ganesh, S.R.G. Naraharisetty, A.K. Chaudhary, S. Srinath, R. Chandrasekar, *J. Mater. Chem. C* (2018) <https://doi.org/10.1039/C8TC02638F>
- S.D. Chemla, J. Zyss, *Nonlinear optical properties of organic molecules and crystals*, Vol. 1. Academic press, Orlando (1987)
- J. Zyss, *Molecular nonlinear optics. Materials, physics and devices*. Academic press, Boston (1994)
- A. Georgieva, N. Mintcheva, N. Trendafilova, M. Mitewa, *Vib Spectrosc* **27**, 153–164 (2001)
- J. Zyss, J. Pecaut, J.P. Levy, R. Masse, *Acta Crystallogr., Sect. B* **49**, 334–342 (1993)
- P.S.P. Silva, M.A.P. Goncalves, M.R. Silva, J.A. Paixao, *Spectrochim. Acta, Part A* **172**, 156–162 (2017)
- K.T. Ma, N. Tin, G.P.A. Thirupathi, D.S. Yap, Richeson, *J. Chem. Soc. Dalton Trans.* (1999) 2947–2951
- C. Cardoso, P.S.P. Silva, M.R. Silva, A.M. Beja, J.A. Paixao, F. Nogueira, A.J.F.N. Sobral, *J. Mol. Struct* **878**, 169–176 (2008)
- P.S.P. Silva, C. Cardoso, M.R. Silva, J.A. Paixao, A.M. Beja, F. Nogueira, *J. Mol. Struct* **888**, 92–98 (2008)
- E. Bravais, *Crystallographiques*, Academie des Sciences, Paris, 1913
- C.F. Macrae, I.J. Bruno, J.A. Chisholm, P.R. Edgington, P. McCabe, E. Pidcock, L. Rodriguez-Monge, R. Taylor, J. Van De Streek, P.A. Wood, *Mercury CSD 2.0-New features for the*

- visualization and investigation of crystal structures. *J. Appl. Crystallogr.* **41**, 466–470 (2008)
24. C.F. Macrae, P.R. Edington, P. McCabe, E. Pidcock, G.P. Shields, R. Taylor, M. Towler, J.V.D. Streek, *J. Appl. Cryst.* **39**, 453 (2006). Mercury (version 1.4.1)
 25. G. SaravanaKumar, P. Murugakoothan, *Spectrochim. Acta, Part A* **131**, 17–21 (2014)
 26. M.S. Kajamuhideen, K. Sethuraman, K. Ramamurthi, P. Ramasamy, *J. Cryst. Growth* **483**, 16–25 (2018)
 27. J. Coates, *Encyclopedia of Analytical chemistry*, John Wiley and sons, (2006) 1–23
 28. N.Y. Maharani, A.C. Peter, S. Gopinath, S. Tamilselvan, M. Vimalan, I.V. Potheher, *J. Mater. Sci.: Mater. Electron.* **27**, 5006 (2016)
 29. T. Balakrishnan, S. Sathiskumar, K. Ramamurthi, S. Thamocharan, *Mat. Chem. Phys* **186**, 115–123 (2017)
 30. K. Nivetha, S. Kalainathan, M. Yamada, Y. Kondo, F. Hamada, *Mat. Chem. Phys* **188**, 131–142 (2017)
 31. M. Bass, *Handbook of optics*. Tata McGraw-Hill companies, inc., vol IV, 5.70–5.83 (2010)
 32. S.S. Priya, A. Alexandar, P. Surendran, A. Lakshman, P. Rameshkumar, P. Sagayaraj, *J. Opt. Mat* **66**, 434–441 (2017)
 33. P. Jayaprakash, M.P. Mohamed, M.L. Caroline, *J. Mol. Struct* **1134**, 67–77 (2017)
 34. R.M. Mohamed, M.K. Mishra, L.M. Al-Harbi, M.S. AlGhamdi, A.M. Asiri, C.M. Reddy, U. Ramamurthy, *Cryst. Growth Des.* **15**, 2479 (2015)
 35. E.M. Onistch, *Mikroskopie*, 2 (1947) 131–151
 36. R. Mekala, R. Mani, I.B. Rietveld, P. Jagdish, R. Mathammal, H. Jiang, *Cryst. Eng. Commun.* **18**, 8194–8206 (2016)
 37. N. Ponpandian, P. Balayya, A. Narayanasamy, *J. Phys.: Condens. Matter* **14**, 3221–3237 (2002)
 38. C.M. Tu, L.H. Chou, Y.C. Chen, P. Huang, M. Rajaboopathi, C.W. Luo, K.H. Wu, V. Krishnakumar, T. Kobayashi, *Opt. Express* **24**, 5039–5044 (2016)
 39. V. Krishnakumar, M. Rajaboopathi, R. Nagalakshmi, *Phys. B* **407**, 1119–1123 (2012)
 40. K. Shanming, H. Haitao, F. Huiqing, *Appl. Phys. Lett.* **89**, 182904–182907 (2006)
 41. L. Zhuo, F. Huiqing, *J. Appl. Phys.* **106**, 054102 (2009)
 42. S.K. Kurtz, T.T. Perry, *J. Appl. Phys.* **39**, 3798 (1968)
 43. M. Krishnakumar, S. Karthick, K. Thirupugalmani, S. Brahadeeswaran, *J. Opt. Mat* **66**, 79–93 (2017)
 44. K. Boopathi, R. Jagan, P. Ramasamy, *Appl. Phys. A* **122**, 1 (2016)
 45. B. Babu, J. Chandrasekaran, R. Thirumurugan, K. Anitha, M. Saravanabhavan, *J. Mater. Sci.: Mater. Electron.* **28**, 9704–9716 (2017)
 46. M.S. Kajamuhideen, K. Sethuraman, K. Ramamurthi, P. Ramasamy, *Opt. Laser. Technol* **91**, 159–165 (2017)
 47. A. Silambarasan, P. Rajesh, P. Ramasamy, *Spectrochimica acta part A: molecular and biomolecular spectroscopy*, 118 (2014) 24–27
 48. N. Vijayan, K. Nagarajan, A.M.Z. Slawin, C.K.S. Nair, G. Bhagavannarayana, *Crystal Growth Des.* **7**, 445–448 (2007)
 49. R. Thirumurugan, K. Anitha, *J. Mol. Struct* **1146**, 273–284 (2017)
 50. J. Jayabharathi, V. Thanikachalam, K. Saravanan, N. Srinivasan, M.V. Perumal, *Spectrochim. Acta A* **78**, 794–802 (2012)
 51. J.F. Nye, *Physical properties of crystals* (Clarendon press, Oxford, 1960)
 52. F. Zernike, J.E. Midwinter, *Applied nonlinear optics* (Wiley, Newyork, 1973)
 53. Y.R. Sharma, *Elementary organic spectroscopic principles and chemical applications* (S. Chand & co, New Delhi, 2004)
 54. D.A. Kleinman, *Phys. Rev.* **126**, 1977–1979 (1962)
 55. H. Chermette, *J. Comput. Chem.* **20**, 129–154 (1999)